

Biological cell (pollen grain) refractive index tomography with digital holographic microscopy

Florian Charrière^a, Etienne Cuche^b, Pierre Marquet^c and Christian Depeursinge^a

^aEcole Polytechnique Fédérale de Lausanne (EPFL), Imaging and Applied Optics Institute, CH-1015 Lausanne, Switzerland, florian.charriere@epfl.ch

^bLyncée Tec SA, PSE-A, CH-1015 Lausanne, Switzerland, www.lynceetec.com;

^cCentre de neurosciences psychiatriques, Département de psychiatrie DP-CHUV, Site de Cery, CH-1008 Prilly-Lausanne, Switzerland

ABSTRACT

This paper presents a novel approach to perform the tomography of biological specimens based on Digital Holographic Microscopy (DHM). A hologram results from the interference between a reference wave and an object wave reflected from or transmitted through a sample. In the hologram, both amplitude and phase of the field transmitted through the object are registered. In DHM, the object field is recovered when the hologram is processed by a digitally computed replica of the reference wave, allowing quantitative measurement of both phase and amplitude. Phase measurements provide high accuracy optical path length measurements across the specimen along the optical axis.

To proceed to a tomographic reconstruction of the refractive index of the sample based on this quantitative phase measurement, such 2-dimensional data must be recorded for different sample orientations covering an angle of 180° to cover all the object spatial frequencies in the reciprocal space. The representation of the data in function of the angle is known as a sinogram. The 3-dimensional refractive index can then be reconstructed from the sinograms by a filtered backprojection algorithm. In our system, the specimen is inserted in a glass micropipette to permit its rotation. To our knowledge, a quantitative tomography of the refractive index of a pollen cell with a resolution in the micron range is presented for the first time.

Keywords: holography, microscopy, phase-contrast, tomography, refractive index, cell imaging

1. INTRODUCTION

Digital holographic Microscopy (DHM) is an imaging modality reconstructing directly the wavefront from a single digitalized hologram in a numerical form. It brings quantitative data derived simultaneously from the amplitude and phase of the complex reconstructed wavefront diffracted by the object and it is used to determine the refractive index and/or shape of the object with accuracy in the nanometer range along the optical axis. DHM comprises a microscope objective to adapt the sampling capacity of the camera to the information content of the hologram.

Since its principle was proposed by Goodman and Lawrence¹ and by Kronrod et al. 30 years ago², digital holographic microscopy (DHM) was developed for a wide range of different applications. In particular, off axis DHM enables to extract both amplitude and phase information of a wave diffracted by a specimen sample from a single hologram^{3,4}. The phase information provides three-dimensional (3D) quantitative mapping of the phase shift induced by microscopic specimens with a resolution along the optical axis better than 1° in some cases, corresponding to 2 nm free wave propagation distance. Thanks to performances of actual personal computers and to the progresses in digital image acquisition, DHM provides nowadays cost-effective instruments for real-time measurements at very high acquisition rates. In a general context, DHM offers numerous operating modes, for instance: tomography on a biological sample performed with wavelength scanning,⁵ investigation of the polarization state of the object using two wave fronts orthogonally polarized,⁶ or multiple wavelength interferometry of dynamic systems.⁷

Digital holographic microscopy (DHM) provides quantitative measurement of the optical path length (OPL) distribution that enable to describe semi-transparent samples, such as living cells with a diffraction-limited transverse resolution and a sub-wavelength axial accuracy.⁸ However, single images as presented in Ref. 8 do not reveal the three-dimensional (3D) internal distribution of cellular components, but a phase shift resulting from a mean refractive index (RI) accumulated over the cellular thickness. We show here that standard optical diffraction tomography (ODT) techniques

can be efficiently applied to reveal internal structures and to measure 3D RI spatial distributions. Pioneer works^{9,10} have established the theoretical basis of reconstructing the 3D scattering potential of weakly scattering objects, by recording the waves scattered from the different directions of parallel illumination. Different techniques have been applied to retrieve the complex waves diffracted by the object, mainly based on phase shifting interferometry (PSI)¹¹ or on phase retrieval algorithms.¹² The illumination direction can be varied by changing the direction of the beam itself,¹¹ or by changing the orientation of the specimen relatively to a fixed illumination beam.¹² The experimental setup used in the present work involves a fixed illumination beam and a rotating sample. The main advantages of DHM for complex diffracted wave retrieval is that only a single hologram is needed for each orientation of the specimen instead of at least 3 images for PSI, reducing the acquisition time and the stability requirements for the system. The biological specimen observed is a yew pollen grain (30 μm diameter), having a 3D-structured nucleus, which makes it an ideal test specimen for the method.

2. METHODOLOGY

2.1 Experimental setup

Transmission DHM (Fig. 1) used for the present study is described in details in Ref. 4. Results presented here have been obtained with a 63X 0.85 NA microscope objective (MO). The light source is a laser diode at 635 nm. The camera is a 512 x 512 pixels, 8 bits, black and white CCD, with square pixels of 6.7 μm , and a maximal frame rate up to 25Hz. The field of view is 80 μm x 80 μm . The transverse resolution (around 1 μm) and the transverse scale calibration are determined with a USAF 1951 resolution test target.

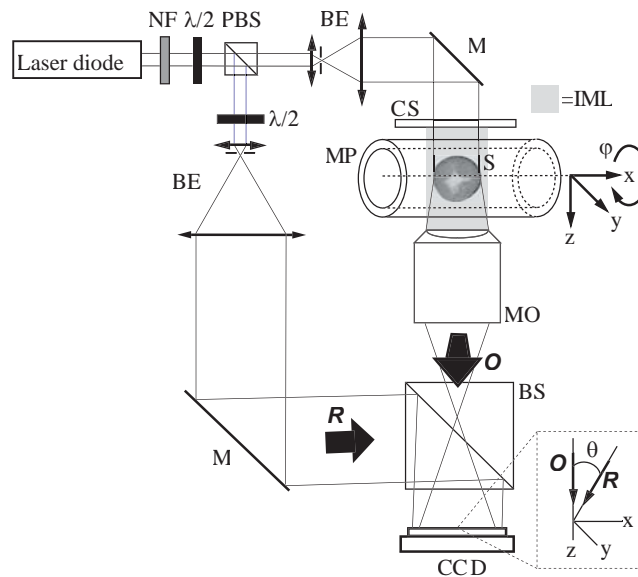


Fig. 1. Digital holographic microscope for transmission imaging: NF neutral density filter; PBS polarizing beam splitter; BE beam expander with spatial filter; $\lambda/2$ half-wave plate; MO microscope objective; M mirror; BS beam splitter; O object wave; R reference wave; MP micropipette; S specimen; IML index matching liquid. Inset: a detail showing the off-axis geometry at the incidence on the CCD.

The pollen cells are in a glass micropipette (MP) filled with a glycerol solution to prevent drying. The MP has an internal diameter of 100 μm , an external diameter of 510 μm , and is fixed on a motorized rotating stage mounted on a micrometric xyz-stage used to center the pollen cell in the field of view. A second xy-stage mounted on the rotating stage itself allows for centering the pollen cell under investigation on the rotation axis, to minimize lateral displacements of the specimen in the field of view during the rotation. The rotation of the stage and the acquisition of

the holograms are controlled with a PC. To minimize strong light refraction by the MP, which acts like a cylindrical lens regarding to the illuminating light, the volume between a glass coverslip and the MO is filled with an index matching fluid suppressing the air/glass interface. The refraction at the MP/glycerol interface is minimal and can be corrected by the numerical adjustment of the reconstruction parameters, as it will be pointed out further.¹³

Measurements presented here have been conducted without any system for insulating against vibrations of the building. This is possible thanks to the remarkably high measurement stability and robustness of DHM, which results from the fact that the off-axis configuration enables to record all necessary information with a single image acquisition of very short duration (a few ms). With a Pentium 4 2.8Ghz, 3D phase reconstruction rate, described in the next chapter, is 15 frames/second.

2.2 Hologram reconstruction

The procedure for hologram processing, in particular for phase reconstruction, is described in details in Refs. 4 and 143-15. For sake of completeness, a short summary is given here. Holograms acquired by the CCD are first submitted to a procedure of apodization¹⁴ and filtered in the Fourier plane in order to remove the zero order and the twin image¹⁵. Then, the resulting hologram I_H , is multiplied by a digital reference wave R_D that simulate an illumination wave^{4,13} and a propagation calculation in the Fresnel approximation is applied to reconstruct a focused image of the specimen in a plane of coordinates $0\xi\eta$, where a digital phase correction $\Phi(m,n)$ is applied to compensate for the wave front curvature induced by the objective lens (see. Refs. 4, 13). In summary, the reconstructed wavefront $\Psi(m\Delta\xi, n\Delta\eta)$, is computed according to the following expression:

$$\Psi(m\Delta\xi, n\Delta\eta) = A\Phi(m,n) \exp\left[\frac{i\pi}{\lambda d} (m^2\Delta\xi^2 + n^2\Delta\eta^2)\right] \times \text{FFT} \left\{ R_D(j,k) I_H(j,k) \exp\left[\frac{i\pi}{\lambda d} (j^2\bar{x}^2 + k^2\bar{y}^2)\right] \right\}_{m,n}, \quad (3)$$

where m and n are integers ($-N/2 \leq m, n < N/2$), FFT is the Fast Fourier Transform operator, $A = \exp(i2\pi d/\lambda)/(i\lambda d)$, $\Delta\xi$ and $\Delta\eta$ are the sampling intervals in the observation plane, \bar{x} and \bar{y} are the pixel size of the CCD. The digital reference wave is computed using the expression of a plane wave

$$R_D(j,k) = \exp\left[i(k_{Dx} \cdot j\bar{x} + k_{Dy} \cdot k\bar{y})\right], \quad (2)$$

where k_{Dx} , and k_{Dy} are the two components of the wave vector. The digital phase correction is computed according to the expression of a parabolic wave front

$$\Phi(m,n) = \exp\left(-i\pi/(\lambda d_1)m^2\Delta\xi^2 - i\pi/(\lambda d_2)n^2\Delta\eta^2\right), \quad (4)$$

where parameters d_1 and d_2 define the field curvature along respectively 0ξ and 0η digitally adjusted to correct the defocusing aberration due to the objective lens. $\Delta\xi$ and $\Delta\eta$ are the sampling intervals in the observation plane.

2.3 Parameters adjustment

Eq. 3 requires the adjustment of four parameters for proper reconstruction of the phase distribution. k_{Dx} and k_{Dy} compensate for the tilt aberration resulting from the off axis geometry or resulting from a not perfect orientation of the specimen surface which should be accurately oriented perpendicular to the optical axis. d_1 and d_2 corrects the wave front curvature according to a parabolic model, in principle these two parameters have very similar values, but it may occur in the presence of astigmatism that better results can be achieved with slightly different values. As explained Ref. 4, the parameters values are adjusted in order to obtain a constant and homogeneous phase distribution on a flat reference surface located in or close to the specimen. With the pollen grain the substrate surrounding the grain (glycerol) is ideal to serve as a reference surface. The manual procedure described in Ref. 4 has been implemented here as a semi automated procedure. First, the program extracts two lines – an horizontal line along 0ξ and a vertical line along 0η – whose location is defined by the operator in the reference surface. Then, one-dimensional (1D) phase data extracted along the two lines are unwrapped¹⁶ in order to remove 2π phase jumps, and a curve fitting procedure is applied to evaluate the unwrapped phase data with a 1D polynomial function of the second order. k_{Dx} and d_1 are iteratively adjusted to minimize the deviation between the fitted curve and the ideal horizontal constant profile. The same way, k_{Dy} and d_2 are adjusted until the vertical profile is as close as possible to the ideal vertical constant profile. In general, less than five iterations are necessary to reach optimal parameters values.

Digital processing of holograms presented in this study is a novel approach in the sense that it performs a numerical reshaping of complex wave fronts and of their propagation, thereby replacing the need of complex optical adjustment procedures. For instance, orienting a mirror or a beam splitter with translation or rotation tables - a task that has to be

performed very accurately in classical interferometry - is simply replaced here by the digital adjustment of the wave vector components k_{Dx} and k_{Dy} . Even more relevant is the digital correction of the wave front deformation induced by the MO.

In the present experiment, this correction of the object wavefront is of particular interest to compensate for the wavefront aberration induced by the micropipette (MP) in which the pollen grain is placed. Despite the use of an index matching liquid surrounding the MP and the presence of high refractive index medium (glycerol, refractive index = 1.47) in the MP, the refractive indices mismatch causes refraction effects on the MP interfaces. Therefore, the MP acts like a cylindrical lens placed in the optical path and distorts consequently the wavefront. On Fig. 2a) is presented the wavefront reconstruction of a typical hologram acquired during this work, when only the tilt, i.e. parameters k_{Dx} , and k_{Dy} , has been adjusted according to above described procedure. The cylindrical phase distortion induced by the MP is clearly apparent. In Fig. 2b), the curvature of the wavefront, i.e. parameters d_1 and d_2 , has also been adjusted to compensate for the cylindrical aberration. Now remains only the phase signal of the pollen grain. This Fig. 2b) also shows, that the phase signal exceeds 2π and that an unwrapping algorithm will be necessarily applied to measure the effective phase shift due to the specimen.

This reconstruction parameters adjustment is of primary importance in all measurements performed with DHM to facilitate the analysis of the phase signal, but in the present study, this adjustment is mandatory. To allow for tomographic reconstruction, several phase images will be acquired and recombined according to a method described in more details further. The perfect removal of the background phase signal is necessary to take into account only the phase signal coming from the specimen under investigation during the tomographic reconstruction.

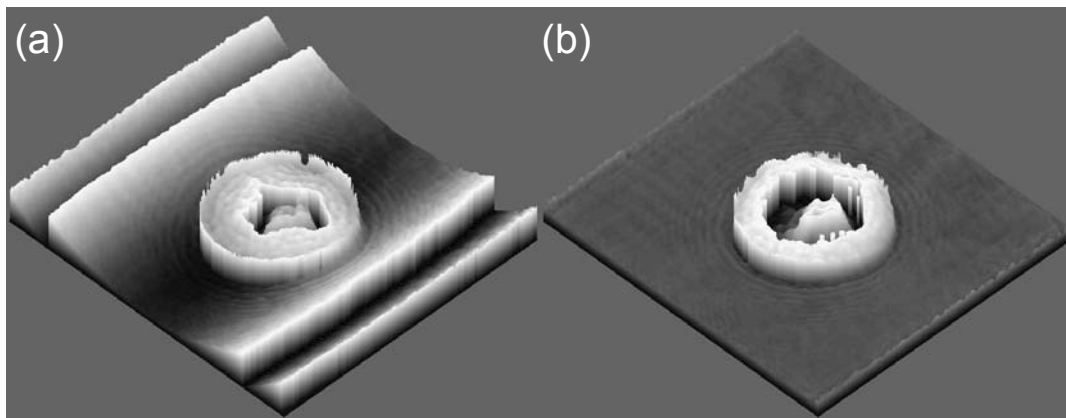


Fig. 2. Reconstructed phase of the pollen specimen without (a) and with the cylindrical aberration compensated by adjustment of the reconstruction parameters (b).

2.5 Performance for phase measurements

DHM provides quantitative phase mapping. In transmission, the phase information, gives the distribution of the optical path length (OPL). The precision for phase measurements, which define the axial resolution of DHM, has been evaluated with two criteria. A first criteria is the spatial standard deviation or spatial root mean square error RMSE, measured over the whole field of view with a flat reference sample. In transmission the spatial RMSE is about 4° , what corresponds to 7 nm in ambient air or to 15.5 nm in a quartz specimen. Secondly the temporal standard deviation, or RMS repeatability, measured for each pixel during 5 minutes, and averaged over the whole field of view is 0.46° , corresponding to 0.8 nm in air or to 1.8 nm in quartz specimens.

Compared to classical phase shifting interferometry, DHM offers similar performances in terms of resolution, precision, repeatability and field of view, and has in addition three main advantages. First measurements are performed much faster, as the complete description of the complex wavefront is obtained from a single hologram capture, while at least three acquisitions are required with phase shifting techniques. This results in a drastically reduced sensitivity to external perturbations (vibration and ambient light), since the capture time is reduced to a few microseconds. Secondly the accuracy of the apparatus is not intrinsically limited by the precision of the control of moving parts, as DHM is exempt

of it. Thirdly the original numerical procedures of DHM for automatic wavefront corrections described in paragraph 2.3 enable a simplification of the optical design.

3. RESULTS: POLLEN GRAIN TOMOGRAPHY WITH DHM

In the case of a weakly diffracting object such as a single biological cell, the optical path length of the collimated illuminating photons across the specimen is parallel to the optical axis.¹⁷ The planar phase distribution $\varphi(x,y)$ provided by DHM is directly proportional to this optical path length. In our experimental setup, the rotation axis is parallel to the x-axis, while the optical axis is the z-axis. $\varphi(x,y)$ can then be expressed as

$$\varphi(x,y) = \int \frac{2\pi}{\lambda} \Delta n(x,y,z) dz, \quad (5)$$

where λ is the wavelength of the light source and $\Delta n(x,y,z)$ is the 3D RI spatial distribution difference between the pollen cell and its surrounding medium. $\varphi(x,y)$ is thus only proportional to the integration of $\Delta n(x,y,z)$ along the z-axis. To proceed to a standard tomographic reconstruction, one must record such 2-dimentionnal (2D) planar phase distribution for different sample orientations covering an angle of 180°. In our study, 90 images were acquired with a 2° step at a rate of 1 Hz. The representation of the data as a function of the angle is known as a sinogram. An example of sinogram is shown on Fig. 3b). Fig. 3a) illustrates one DHM phase image of the pollen grain, corresponding to the 62° measurement. The dashed line drawn on Fig. 3a), defining a cut in the pollen grain perpendicular to its rotation axis, is represented in the sinogram in function of the rotation of the grain.

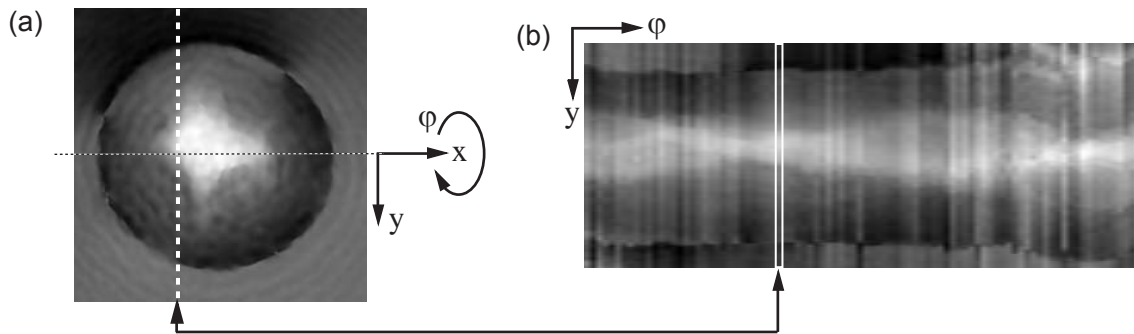


Fig. 3. DHM phase image of the pollen cell with a 62° orientation (1), sinogram of a given pollen slice (dashed line on (1))

The 3D signal $\Delta n(x,y,z)$ can be reconstructed from the sinograms by a filtered backprojection algorithm (see for ex. Ref. 18). For this purpose, the standard inverse radon transform *iradon* from the Matlab programming environment was used in a slice-by-slice implementation. The use of filtered backprojection algorithm instead of backpropagation¹⁹ algorithm usually recommended in ODT is consistent with the assumption of a phase proportional to the optical path length across the specimen. The maximal spatial resolution of $\Delta n(x,y,z)$ depends on the sampling step used to cover the 180° during the rotation of the specimen and on the spatial resolution of $\varphi(x,y)$. The 2° step used in this study is sufficient for the maximal spatial resolution to be reached.

The reconstruction is summarized on Fig. 2. Fig. 2.1 illustrates a cut in the 3D function $\Delta n(x,y,z)$ along the xy-plane in the middle of the pollen cell, while Fig. 2.2 and 2.3 show cuts at different positions in the cell along the yz-plane and the xz-plane respectively. On this figure, one can appreciate the 3D structure of the nucleus of the pollen grain. Knowing that the RI of the glycerol surrounding the pollen is 1.473, a $\Delta n=0.06\pm 0.01$ is measured in the nucleus, leading to a measured value of 1.53. The RI of the pollen wall, around 1 μm thick, is not clearly measurable in the present study. The pollen cells possess a resistant wall layer or exine outside the usual cell wall, which is chemically resistant to minimize damage and prevent drying of the cell. The exine is composed of a group of substances called sporopollenins, which include polymers of mono- or di-carboxylic fatty acids of high molecular weight organized in a complex structure. The internal cell wall, or intine, is formed by cellulose, pectic substances, callose, and other polysaccharides. The presence of these components involves an important refractive index value, all of them having a refractive index above 1.50, and therefore an abrupt phase shift $\Delta\varphi$ between the glycerol and the cell wall. Our hypothesis of a weakly

diffracting object might not be entirely fulfilled with this important RI change in the pollen wall, but as it is very localized (around $1\ \mu\text{m}$), this assumption remains at least perfectly valid for the rest of the pollen grain. Furthermore, as the wall thickness is comparable to the lateral resolution of the system, difficulties appear during the unwrapping procedure involved in the reconstruction process to avoid 2π -jumps in the phase signal, leading to some discrepancies in the phase measurement from an image to another for this critical part of the cell. An increase of the lateral resolution of the system or an adaptation of the embedding medium RI should improve the reliability of the reconstructed phase images. Secondly, the rotation system induces small movements (few microns range). Even if a numerical procedure based on the center of mass determination was used to re-center the cell on its rotation axis, the accuracy of this procedure was also limited to about $1\ \mu\text{m}$, making the tomographic reconstruction of this around $1\ \mu\text{m}$ -thick wall difficult. The slowly varying RI of the $12\ \mu\text{m}$ nucleus is not affected by the two artifacts described above.

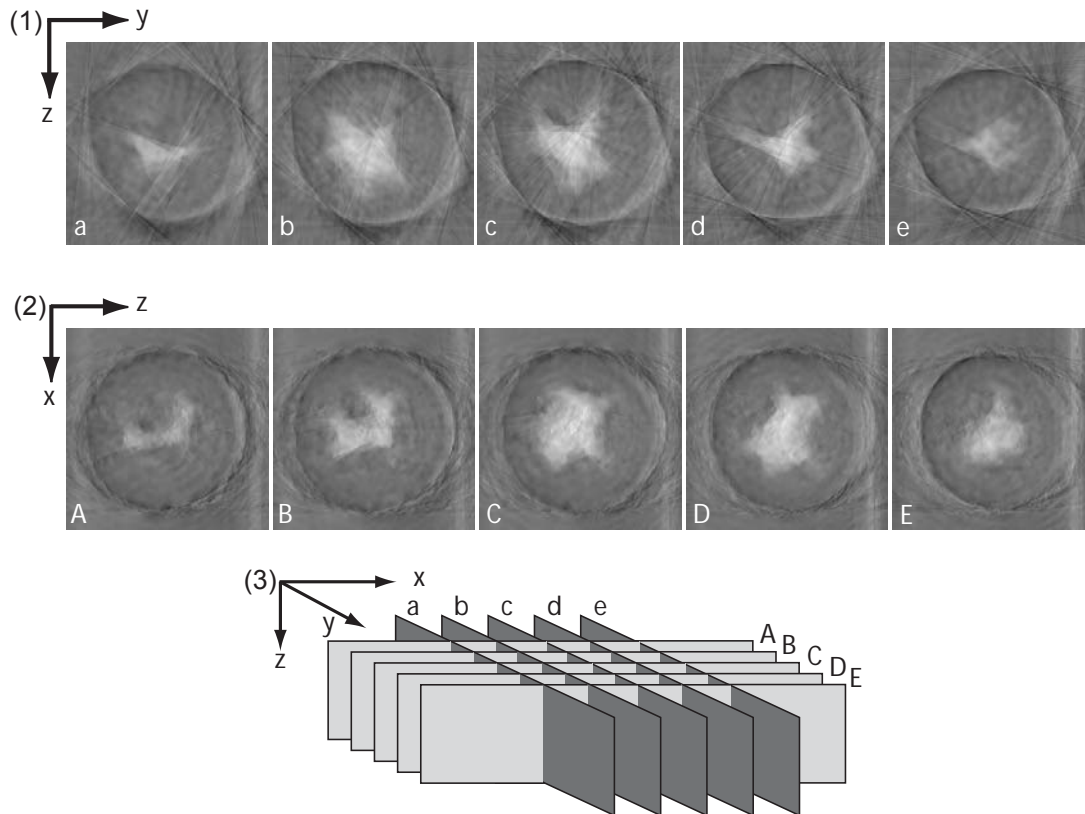


Fig. 4. Tomography of a pollen cell refractive index: cuts at different positions in the cell resp. along the yz-plane (1) and the xz-plane (2), schematic of the presented cuts (3). The cuts are distant of 2.5 microns from each other.

Recently, a comparative method between height measurement with confocal microscopy and OPL determination with a phase-sensitive technique²⁰ has shown an accuracy of 0.004 in the measurement of the integrated RI through a muscle cell, but request the use of two different setups and therefore specimen manipulation. This kind of approach is not able to separate the RI of the different cell constituents, as it only measures an integrated value. The tomography presented here of course overcomes this drawback, and provides 3D RI distributions.

The knowledge of the 3D RI spatial distribution of a cell leads to invaluable information concerning the distribution and the optical properties of the intracellular organelles. In spite of this major issue, ODT applied successfully to cell imaging has to our knowledge not provided quantitative results till today.^{11,21} Reliable RI values are difficult to obtain from the literature as different measuring techniques were applied on different type of cells. A good review of the

available techniques and refractive indices in the literature can be found in Ref. 22. Most of the presented techniques are designed to evaluate the RI of a specific cell component (membrane, nucleus, cytoplasm...) and in this sense, the method we propose is more general as it furnishes a complete 3D distribution of the RI in the cell. In this review also, the values of RI for the different components of the cell are given with 0.01 accuracy, making our setup already competitive regarding to other available methods. Furthermore, ODT of optical fibers based on the same specimen rotation principle presented here has already shown RI measurements with accuracy of 0.001.¹² In spite of the accurate results obtained with optical fibers, this technique has to our knowledge never been applied to biological specimen. With a specifically designed mechanical system avoiding any movement, or an appropriate re-centering numerical procedure, ODT based on DHM should aim the same precision in the RI measurement thanks to the nanometric sensitivity in the phase determination.

4. CONCLUSION

In conclusion, we have shown for the first time to our knowledge the 3D distribution of RI of a semi-transparent object, in our case a pollen grain, provided by backprojecting OPL values collected with DHM on a series of projections of the preparation taken at various incidence angles. The accuracy of the RI determination is better than 0.01 and the 3D spatial resolution is better than 1 μm in all 3D. This approach could find interesting application as a reference measuring technique in material and life sciences.

ACKNOWLEDGEMENTS

This research has been supported by the Swiss National Science Foundation (SNSF) grant 205320-103885/1. The authors thank Benoît Gerber for his participation to the work. Florian Charrière's email is florian.charriere@a3.epfl.ch.

REFERENCES

1. J.W. Goodman and R.W. Lawrence, "Digital Image Formation from Electronically Detected Holograms," *Applied Physics Letters* 11, 77-& (1967).
2. M.A. Kronrod, N.S. Merzlyakov, and L.P. Yaroslavskii, "Reconstruction of a hologram with a computer," *Sov. Phys. Tech. Phys.* 17, 333-334 (1972).
3. E. Cuche, *Numerical reconstruction of digital holograms: application to phase-contrast imaging and microscopy* (Ecole Polytechnique Fédérale de Lausanne EPFL, Lausanne, 2000).
4. E. Cuche, P. Marquet and C. Depeursinge, "Simultaneous amplitude and quantitative phase-contrast microscopy by numerical reconstruction of Fresnel off-axis holograms," *Appl. Opt.*, 38, 6994-7001 (1999).
5. M.K. Kim, "Tomographic three-dimensional imaging of a biological specimen using wavelength-scanning digital interference holography," *Optics Express*, 7, 305-310 (2000).
6. T. Colomb, E. Cuche, F. Montfort, P. Marquet, and C. Depeursinge, "Jones vector imaging by use of digital holography: simulation and experimentation," *Optics Communications*, 231, 137-147 (2004).
7. N. Demoli, D. Vukicevic, and M. Torzynski, "Dynamic digital holographic interferometry with three wavelengths," *Optics Express*, 11, 767-774 (2003).
8. P. Marquet, B. Rappaz, P. J. Magistretti, E. Cuche, Y. Emery, T. Colomb and C. Depeursinge, "Digital holographic microscopy: a noninvasive contrast imaging technique allowing quantitative visualization of living cells with subwavelength axial accuracy", *Opt. Lett.*, 30, 468-470 (2005).
9. E. Wolf, "Three-dimensional structure determination of semi-transparent object from holographic data, " *Opt. Comm.*, 1, 153-156 (1969).
10. R. Dändliker, K. Weiss, "Reconstruction of three-dimensional refractive index from scattered waves, " *Opt. Comm.*, 1, 323-328 (1970).
11. V. Lauer, "New approach to optical diffraction tomography yielding a vector equation of diffraction tomography and a novel tomographic microscope," *J. Microsc.*, 205, 165-176 (2002).
12. A. Barty, K.A. Nugent, A. Roberts, D. Paganin, "Quantitative phase tomography," *Opt. Comm.*, 175, 329-336 (2000).

13. T. Colomb, E. CuChe, F. Charrière, J. Kühn, N. Aspert, F. Montfort, P. Marquet, and C. Depeursinge, "Automatic procedure for aberrations compensation in digital holographic microscopy and applications to specimen shape compensation," *Appl. Opt. Digital Holography*, to be published Feb. 2006.
14. E. CuChe, P. Marquet, and C. Depeursinge, "Aperture apodization using cubic spline interpolation: application in digital holographic microscopy," *Optics Communications*, 182, 59-69 (2000).
15. E. CuChe, P. Marquet, and C. Depeursinge, "Spatial filtering for zero-order and twin-image elimination in digital off-axis holography," *Appl. Opt.*, 39, 4070-4075 (2000).
16. H. Takajo and T. Takahashi, "Noniterative method for obtaining the exact solution for the normal equation in least-squares phase estimation from the phase difference," *J. Opt. Soc. Am. A*, 5, 1818-1827 (1988).
17. P. Marquet, "Développement d'une nouvelle technique de microscopie optique tridimensionnelle, la microscopie holographique digitale. Perspective pour l'étude de la plasticité neuronale," MD-PhD Thesis Dissertation (Chapt. 5), UNI-Lausanne, 2003.
18. A. C. Kak and M. Slaney. *Principles of Computerized Tomographic Imaging*. Soc. of Ind. and Appl. Math. SIAM, 2001.
19. T. C. Wedberg, J. J. Stamnes and W. Singer, "Experimental examination of the quantitative imaging properties of optical diffraction tomography," *Appl. Opt.*, 34, 6575-6581 (1995).
20. C. L. Curl, C. J. Bellair, T. Harris, B. E. Allman, P. J. Harris, A. G. Stewart, A. Roberts, K. A. Nugent and L. M. D. Delbridge, "Refractive index measurement in viable cells using quantitative phase-amplitude microscopy and confocal microscopy", *Cyt. A*, 65, 88 (2005).
21. T. Noda, S. Kawata and S. Minami, "Three-dimensional phase-contrast imaging by a computed-tomography microscope", *Appl. Opt.*, 31, 670-674 (1992).
22. A. Dunn, *Light scattering properties of cells*, PhD Diss., Univ. of Texas, Austin, 1997.